BBA - Proteins and Proteomics 1866 (2018) 933–940

Contents lists available at ScienceDirect

BBA - Proteins and Proteomics

journal homepage: www.elsevier.com/locate/bbapap

The role of extended Fe_4S_4 cluster ligands in mediating sulfite reductase hemoprotein activity

Marisa R. Cepeda[a,b,1], Lauren McGarry[a,1], Joseph M. Pennington[a], J. Krzystek[c], M. Elizabeth Stroupe[a,*]

[a] Department of Biological Science, Institute of Molecular Biophysics, Florida State University, Tallahassee, FL 32306, USA
[b] Department of Biological Sciences, Georgia Institute of Technology, 310 Ferst Dr. NW, Atlanta, CA 30332, USA
[c] National High Magnetic Field Laboratory, Florida State University, Tallahassee, FL 32310, USA

ARTICLE INFO

Keywords:
Redox enzyme
Metalloenzyme
Sulfite reductase hemoprotein
Iron-sulfur cluster

ABSTRACT

The siroheme-containing subunit from the multimeric hemoflavoprotein NADPH-dependent sulfite reductase (SiR/SiRHP) catalyzes the six electron-reduction of SO_3^{2-} to S^{2-}. Siroheme is an iron-containing isobacteriochlorin that is found in sulfite and homologous siroheme-containing nitrite reductases. Siroheme does not work alone but is covalently coupled to a Fe_4S_4 cluster through one of the cluster's ligands. One long-standing hypothesis predicted from this observation is that the environment of one iron-containing cofactor influences the properties of the other. We tested this hypothesis by identifying three amino acids (F437, M444, and T477) that interact with the Fe_4S_4 cluster and probing the effect of altering them to alanine on the function and structure of the resulting enzymes by use of activity assays, X-ray crystallographic analysis, and EPR spectroscopy. We showed that F437 and M444 gate access for electron transfer to the siroheme-cluster assembly and the direct hydrogen bond between T477 and one of the cluster sulfides is important for determining the geometry of the siroheme active site.

1. Introduction

Metallic cofactors enhance proteins' catalytic repertoire, including their ability to perform redox chemical reactions. For example, biological reduction of sulfur or nitrogen from S^{4+} to S^{2-} or N^{3+} to N^{3-} depends largely on two homologous metalloenzymes called siroheme-dependent sulfite or nitrite reductase hemoprotein (S/NiRHP) [1]. S/NiRHPs use an iron-containing porphyrinoid (siroheme) that is covalently coupled to a Fe_4S_4 cluster through a mutual cysteine ligand to perform these six-electron reductions [2], the only known biological reduction of such magnitude to a single atom acceptor. Six-electron nitrogen reduction can also be catalyzed by a multi-heme metalloenzyme [3]. Siroheme-dependent SiRHP is, with few known exceptions [4,5], the predominant enzyme fold used across a wide range of biological niches from sulfur-based respiration (dissimilatory sulfur reduction) to metabolic sulfur reduction for incorporation into biomolecules like cysteine and methionine (assimilatory sulfur reduction) (Fig. 1).

In α-proteobacteria like *Escherichia coli*, SiRHP is one subunit of an ~800 kDa sulfite reductase holoenzyme (SiR) that includes an octamer of cytochrome *p*450 reductase-like NADPH-dependent flavoprotein (SiRFP) subunits, which collectively bind to four SiRHP enzymes [8]. Full length SiRFP forms an octamer when expressed alone whereas full length SiRHP is a monomer when expressed alone [9]. The nature of the dodecameric complex remains something of a mystery. Nevertheless, we know that the N-terminus of SiRFP is important for octamerization and the N-terminus of SiRHP is important for complex formation with its reductase subunit [10]. Other assimilatory sulfite reductases (aSiRs) from organisms like *Mycobacterium tuberculosis* and the *Zea mays* chloroplast use a transiently interacting ferredoxin partner to the monomeric hemoprotein, as do some dissimilatory sulfite reductases (DSR) (Fig. 1A) [1]. Other DSRs have unknown reductase partners but contain a ferredoxin insertion domain that may facilitate that function [11].

The coupled iron center in SiRHP is evolved to process a high number of electron transfers to a changing substrate, seeming to occur one at a time through a push-pull mechanism in concert with proton donation by structurally-bound waters and key amino acids in the active site [12]. SiRHP can exist in three functionally important oxidation states: fully oxidized ($Fe^{3+}/Fe_4S_4^{2+}$); partially reduced ($Fe^{2+}/Fe_4S_4^{2+}$; and fully reduced ($Fe^{2+}/Fe_4S_4^{1+}$) [13–15]. The siroheme and Fe_4S_4 cluster are covalently linked through a shared cysteine ligand that

* Corresponding author.
[1] These authors contributed equally to this work.

https://doi.org/10.1016/j.bbapap.2018.05.013
Received 12 January 2018; Received in revised form 8 May 2018; Accepted 24 May 2018
Available online 28 May 2018

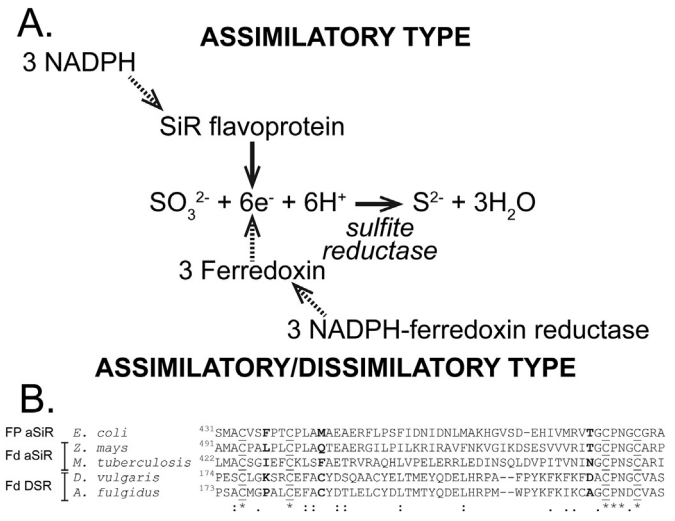

Fig. 1. Sulfite reduction by assimilatory sulfite reductase A. Assimilatory sulfite reductase hemoprotein catalyzes the six-electron reduction of sulfite to sulfide, either using an NADPH-dependent flavoprotein or ferredoxin reductase partner. B. Conservation of F437, M444, and T477 across ferredoxin-dependent assimilatory SiRHP or dissimilatory SiRHPs. *Indicates perfect conservation between the *Esherichia coli*, *Zea mays*, *Mycobacterium tuberculosis*, *Desulfovibrio vulgaris*, and *Archeoglobus fulgidus* SiRHPs. :Indicates strong similarity between amino acids and .indicates weak similarity, as aligned in Clustal Omega [6,7].

couples the oxidation state of the cofactors in a way that is unique to this multi-iron prosthetic group [13] but is not fully understood. Specifically, how the environment of the Fe_4S_4 simultaneously influences formation of a productive electron transfer complex and the active site geometry at the distal face of the siroheme is not known.

Multi-atom Fe-S clusters generally bind to protein scaffolds through cysteine or histidine ligands, so the task of fine-tuning their properties falls to second shell ligands that surround the cluster-binding loops. In the case of SiRHP, 3 s shell ligands are unique because of their proximity to the four cysteine ligands that bind the Fe_4S_4 cluster [2]. First, a surface phenylalanine, F437, caps the first cluster loop (amino acids C434 to C440) and is solvent exposed, leading to the prediction that it could play a role in electron transfer from SiRFP or in subunit-subunit binding. Second, a surface methionine, M444, interacts with C479 Cβ, one of the cluster ligands, effectively shielding the cluster from solvent. Third, T477 forms a direct hydrogen bond with one of the sulfur ions in the iron sulfur cluster. The conservation pattern of these amino acids differs across homologs, suggesting they assume specific roles in NADPH-dependent, assimilatory SiR (Fig. 1B).

We explored the impact of each functional group on the structure and activity of *E. coli* SiRHP to gain insight into the mechanism by which the SiRHP protein harnesses the reactivity of the Fe_4S_4 cluster. We generated single alanine alterations at amino acids 437, 444, and 477, and then expressed and purified the altered proteins as monomeric SiRHP or as part of the dodecameric SiR. Then, we characterized the structure, activity, spectroscopic behavior, and electron paramagnetic resonance (EPR) properties of each. Our results showed that the two large substituents, F437 and M444, play a role in gating electron transfer to the active site whereas T477 plays a role in setting the geometry of the active site, far from the point of amino acid alteration.

2. Materials and methods

2.1. Point variant synthesis, purification, and analysis

Point mutations were introduced into the *cysI* gene either as part of the untagged SiRHP or as N-terminally six-histidine (his)-tagged SiRFP + untagged SiRHP pBAD expression vectors that both co-express *cysG* to ensure sufficient siroheme synthesis [10,12,16] by use of QuikChange PCR reactions [17] with the following primers and their reverse complements: F437A - caatggccTGCgtgtcattcccgacttgcccgctg, M444A - cttgcccgctggcgGCGgcggaagcggagc, and T477A - cgtgatgcgtgtaGCAggctgcccgaacggttg. Changes were confirmed with sequencing (Eurofins Genomics, Louisville, KY, USA). Untagged SiRHP, his-tagged SiR, or an N-terminally-truncated monomeric SiRFP of 43 kDa in mass (SiRFP-43) was purified after overexpression in LMG194 *E. coli* supplemented with ampicillin for pBAD selection, as previously described [10,12]. Extinction coefficients for each variant were assessed by use of bicinchoninic acid (BCA) detection (Millipore-Sigma, St. Louis, MO, USA) for determining independent protein concentrations for each variant. SDS-PAGE and UV–Visible (UV–Vis) spectroscopy was used to assess the purity and stability of our protein preparations.

Native blue gel electrophoresis was used to assess the ability of each SiRHP variant to bind SiRFP. We used an N-terminally truncated monomeric form of SiRFP (SiRFP-43) to simplify the experiment, knowing that it binds SiRHP with similar affinity to wild-type enzyme (WT) [10]. Two-fold excess SiRFP-43 was mixed with SiRHP variants and incubated for 30 min on ice before being mixed with non-denaturing loading dye and loaded onto a 4–16% gradient NativePAGE Bis-Tris Protein Gel (ThermoFisher Scientific, Waltham, MA, USA).

2.2. Complementation assays

SiRHP-deficient *E. coli* (*cysI*$^-$, Keio strain JW2733 [18]) can be rescued for survival in sulfur-limited growth conditions by replacement with a functional SiRHP-expressing gene supplied on an exogenous plasmid. We transformed this strain with WT SiRHP, empty, or variant SiRHP expression vectors. After overnight growth in lysogeny broth (LB) supplemented with ampicillin (pBAD selection) and kanamycin (JW2733 selection), cells were carefully washed in 1 × M9 salts and the concentration of cells for each culture was normalized based on their scattering at 600 nm. Cells were then plated as serial dilutions on either LB or M9 media, which only supplied SO_4^{2-} (S^{6+}) so required functional SiRHP to survive. The colony diameters were measured from digitized scans of the M9 plates where each plate contained each experimental condition to control for possible differences in growth conditions by use of the ImageJ software [19,20] and reported in terms of % WT size. Pairwise *t*-tests were performed in Excel (Microsoft, Redmond, WA, USA).

2.3. SiRHP/SiR activity assays

Activity of isolated, monomeric SiRHP was measured by monitoring its ability to oxidize the chemical reductant methyl viologen (MV^+), which results in a decrease in absorbance at 604 nm (ε = 13,000 M^{-1} cm^{-1}) [12,14]. Activity of dodecameric SiR was measured by monitoring a decrease in NADPH absorbance at 340 nm upon oxidation to $NADP^+$ (ε = 6220 M^{-1} cm^{-1}) on an Agilent 8453 spectrophotometer (Agilent Technologies, Santa Clara, CA, USA) [10,21]. Stock solutions of 0.5 M HCl, 1 M potassium phosphate buffer (KP_i), pH 7.8, and 0.5 M EDTA, pH 8.0 were purged with N_2 gas under vacuum before being imported into a UNIlab anaerobic chamber (mBRAUN, Stratham, NH, USA) under a nitrogen gas atmosphere.

Reaction mixtures for monitoring SiRHP activity were prepared anaerobically in 1 cm path length septum-sealed quartz cuvettes. Each 1 mL sample contained 100 mM KP_i, pH 7.8, 1 mM SO_3^{2-}, 150 μM Cr (II) EDTA, and 100 μM MV^+. The reaction was initiated after injection of 5 μL of 0.5 mg/mL SiRHP into each mixture. Reactions mixtures for monitoring SiR activity were also prepared in 1 cm path length septum-sealed quartz cuvettes. Reactions of 100 mM KP_i, pH 7.8, 200 μM NADPH, 80 μM $NaHSO_3$, 10 mM glucose, and 10 units of glucose oxidase were prepared and the reaction was initiated by injection of 5 μL of 0.2 mg/mL SiR *via* a gastight syringe. Background measurements were simultaneously made on reactions mixtures that were initiated by

Table 1
Data collection and refinement statistics.

	Wild-type	F437A	M444A	T477A
Data collection				
Space group	$P2_12_12_1$	$P2_12_12_1$	$P2_12_12_1$	$P2_12_12_1$
Unit cell dimensions (Å)	68.4, 77.2, 87.2	68.8, 77.3, 87.6	67.8, 77.3, 87.6	68.2, 77.3, 87.3
α, β, γ (°)	90, 90, 90	90, 90, 90	90, 90, 90	90, 90, 90
Resolution (Å)	35.3–1.54 (1.60–1.54)	35.4–1.54 (1.60–1.54)	35.4–1.54 (1.60–1.54)	35.4–1.68 (1.74–1.68)
R_{pim}	0.121 (1.65)	0.0558 (0.397)	0.0823 (0.528)	0.0482 (0.931)
$I/\sigma I$	15.2 (1.5)	22.7 (3.7)	13.9 (1.6)	13.2 (0.6)
Completeness (%)	99.4 (95.8)	99.5 (94.9)	97.8 (84.2)	74.7 (19.1)
	13.2 (3.8)	13.2 (5.7)	10.6 (2.8)	11.2 (2.6)
Refinement				
Resolution (Å)	35.3–1.54 (1.60–1.54)	35.4–1.54 (1.60–1.54)	35.4–1.54 (1.60–1.54)	35.4–1.94 (2.0–1.94)
No. reflections	68,383 (6514)	69,151 (6536)	67,052 (5732)	39,731 (2597)
R_{work}	0.155 (0.251)	0.142 (0.167)	0.157 (0.280)	0.189 (0.294)
R_{free}	0.177 (0.283)	0.164 (0.179)	0.190 (0.287)	0.248 (0.314)
No. atoms	4292	4468	4388	4065
Protein	3671	3786	3795	3723
Ligand/ion	77	77	77	77
Water	544	605	516	265
B-factors (Å^2)				
Protein	22.42	15.98	19.01	37.14
Ligand/ion	14.98	9.7	11.84	32.56
Water	38.02	30.52	34.15	39.9
R.m.s. deviations				
Bond lengths (Å)	0.008	0.009	0.009	0.008
Bond angles (°)	1.51	1.54	1.48	1.28

injection of 5 µL of buffer rather than protein solution. For specific activity calculations, SiRHP concentration was determined from the siroheme Q-band absorbance at 590 nm.

2.4. X-ray crystallographic analysis

Purified SiRHP proteins treated with trypsin to remove the N-terminal 60 amino acids for crystallization in 65 mM KP_i, 15–20% polyethylene glycol 8000, and 1 mM EDTA as previously described [2]. Crystals were stabilized in 12% glycerol for flash freezing. X-ray diffraction data was collected on beamline 22-ID at the Advanced Photon Source at 1 Å wavelength. Initial phases were determined by molecular replacement against the WT structure (PDB ID: 1AOP [2]) and refined with manual fitting in COOT [22] and energy minimization in PHENIX [23] (Table 1).

2.5. EPR analysis

210 µM solutions of SiRHP variants in 100 mM KP_i, pH 7.8, 1 mM EDTA were slow cooled in liquid nitrogen before introduction to the cavity of the E680X X-band EPR spectrometer (Bruker, Billerica, MA, USA). The temperature of the experiment was controlled by an E900 cryostat (Oxford Instruments, Abingdon, UK) and the EPR spectrum for each variant was measured at 10 and 20 K with 10 and 20 dB power attenuation and sweeping the field up or down in the range from 850 to 3850 G to account for a slight instrumental hysteresis. The spectra were subsequently simulated using the program SPIN to assess the g-values.

2.6. UV–Vis spectroscopy of reduced CN^--bound SiRHP variants

Purified SiRHP samples in 100 mM KP_i, pH 7.8 and 1 mM EDTA were degassed by gently bubbling the protein solution with N_2 gas before moving the samples into an anaerobic chamber (mBRAUN, Stratham, NH, USA). SiRHP was reduced with Cr(II)-EDTA/MV^+ as previously described [12] with the addition of 10 mM KCN. After 30 min, the mixture was desalted over a PD-10 G-25 desalting column (GE Healthcare, Little Chalfont, UK) previously equilibrated in anaerobic buffer. CN^--bound SiRHP was concentrated using a 10 K MWCO concentrator before moving the sample to a septum-sealed quartz cuvette. UV–Vis spectra were measured on an Agilent 8453 spectrophotometer (Agilent Technologies, Santa Clara, CA, USA) using the concentration flowthrough as a blank, removing absorbance from trace Cr-EDTA/MV. All measurements were repeated in triplicate for each SiRHP variant.

3. Results

3.1. Amino acid variant generation and complementation analysis

We used QuikChange mutagenesis to alter the SiRHP gene, *cysI*, at the codons encoding amino acids F437, M444, or T477 to alanine. We then transformed *cysI*$^-$ *E. coli* with WT, F437A, M444A, T477A, or empty pBAD plasmid and probed the ability of each variant to catalyze the reduction of sulfite to sulfide *in vivo* by screening on M9 minimal media that required transformation of SO_4^{2-} to SO_3^{2-}, then to S^{2-} by SiR, for growth. Each of the variants complemented the SiRHP deficiency, showing that none of the amino acids we targeted were essential for activity (Fig. 2A). Nevertheless, we noticed that the individual colonies from the cell-number normalized serial dilutions appeared smaller so we measured and compared the diameter of the colonies for the WT-, F437A-, M444A-, or T477A-expressing bacteria, which were reduced by 40–60% from WT (Fig. 2B).

UV–Vis spectroscopic analysis is a strong measure of the purity and integrity of SiRHP because of its unique optical spectrum that indicates the ratio of protein (A_{280}) to siroheme (A_{389}) and flavin contact (A_{455}). UV–Vis spectra of WT and the three point variants show the integrity of our sample preparations (Fig. 3A). Further, none of the variants were deficient in their ability to bind SiRFP, as judged by native blue gel electrophoresis (Fig. 3B). SiRFP-43 ran as a single species at the anticipated 43 kDa mass but SiRHP ran slightly higher than the expected 64 kDa mass. When mixed with two-fold excess SiRFP, all of the SiRHP shifted into the heterodimeric form that ran at about 100 kDa.

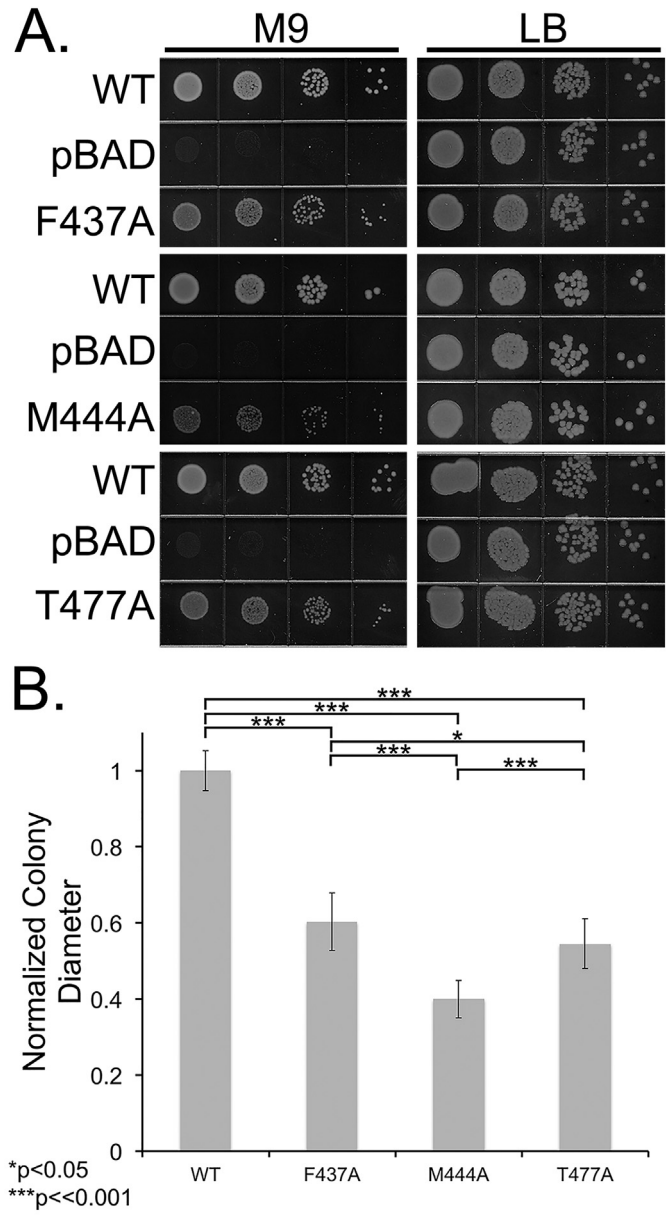

Fig. 2. Complementation of SiRHP-deficient *E. coli* by SiRHP and variants. A. M9 or control LB media both support growth of SiRHP-deficient *E. coli*, but the F437A, M444A, and T477A point variants result in less robust bacterial growth on the selective media. B. Analysis of the colony width showed the smaller colonies are statistically significant.

3.2. Activity assays

Knowing that each SiRHP variant was active for sulfite reduction in the complementation assays, we next asked how their specific activity compared to WT. We performed activity assays in two different ways to test two aspects of SiRHP catalysis. First, we overexpressed purified, monomeric SiRHP from the above pBAD expression system. In this assay, we provided reducing equivalents chemically in the form of MV^{+} and monitored activity spectroscopically, keeping track of MV^{+} oxidation to MV^{2+} as it reduced SiRHP for sulfide synthesis. By this assay, each of the point variants was more active than the WT enzyme (Table 2).

We next wanted to know if this trend was reproduced in the SiR holoenzyme so we generated the point variants in our SiR pBAD expression construct that expresses both SiR subunits, along with CysG, to make the dodecameric complex. As in monomeric SiRHP, the F437A and T477A SiR variant activities were higher than the WT enzyme (Table 2). In contrast, the M444A SiR variant was not.

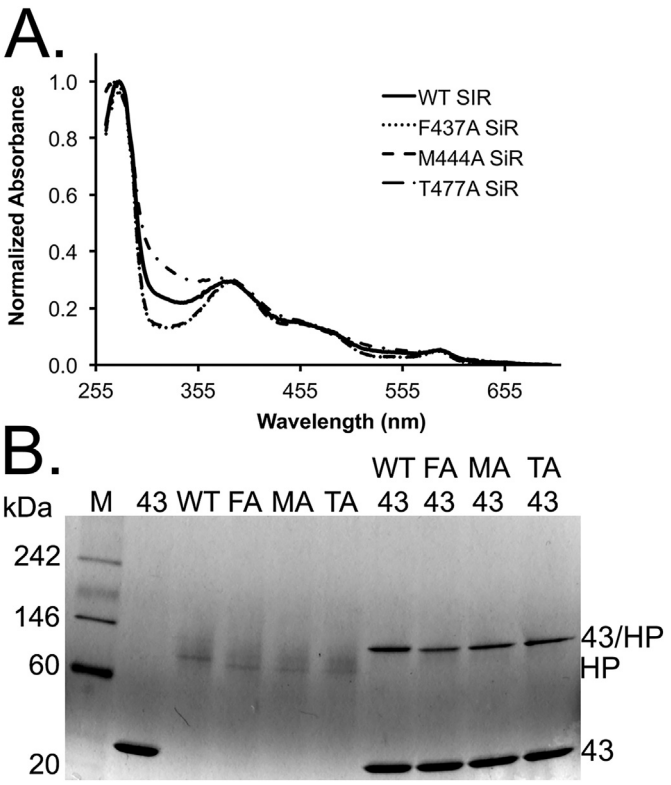

Fig. 3. Analysis of the point variants shows they all form the SiR holoenzyme. A. UV–Vis spectroscopy shows the proper cofactor occupancy for each variant. B. Native-blue gel analysis shows that the point variants do not affect SiRFP-43/SiRHP binding. 43 = SiRFP-43 WT = wildtype SiRHP, FA = F437A SiRHP, MA = M444A SiRHP, TA = T477A. (For interpretation of the references to colour in this figure legend, the reader is referred to the web version of this article.)

3.3. X-ray crystallographic analysis

We wanted to know if altering tehse amino acids significantly altered the structure of SiRHP, so we determined their structures by use of X-ray crystallography. Increased power of synchrotron radiation over the 20 years since determining the original X-ray structure can reduce heme centers *via* cryoradiolytic reduction [24]. Therefore, we also determined the WT enzyme structure so we could directly compare the quality of the electron density of each variant to that structure. In the original structure of SiRHP, the iron is domed by 0.3 Å above the plane of the pyrrole nitrogens [25] whereas in each of the new structures, the iron moved into the plane of the pyrrole nitrogens without loss of the distally bound PO_4^{2-}, consistent with reduction (Fig. 4).

Despite their proximity to the Fe_4S_4 cluster, none of the point variants significantly altered the strained geometry in the first cluster loop (Fig. 4, stick drawing). Not surprisingly, however, removal of the bulky phenylalanine or methionine side chains altered the solvent accessible surface around the Fe_4S_4 cluster (amino acids A433-A445), reducing the volume enclosed in that region from 59,340 $Å^3$ in the WT enzyme to 59,220 $Å^3$ for both F437A and M444A (Table 2). T477A is on the other side of the cluster from this loop and its alteration does not dramatically affect this area (Table 2). Further, the F437A variation increased the solvent accessible surface of this loop, from 18,130 $Å^2$ to 18,260 $Å^2$ (Table 2).

In the WT enzyme and the other two non-F437 point variants, the presence of the bulky hydrophobic phenyl substituent excludes water molecules in the immediate vicinity of the first cluster-binding loop. In

Table 2
Activity measurements and structure analysis of SiRHP and its variants.

	WT	F437A	M444A	T477A
Specific activity (SiRHP) (MV^+ min^{-1} $siroheme^{-1}$)	810 ± 90	1800 ± 80	1600 ± 130	1300 ± 190
Specific activity (SiR holoenzyme) (NADPH min^{-1} $siroheme^{-1}$)	260 ± 8	520 ± 20	170 ± 10	530 ± 20
Volume A433-A445 (Å^3)	59,340	59,220	59,220	59,310
Area A433-A445 (Å^2)	18,130	18,260	18,190	18,170
C483Sγ to SRM-FE (Å)	2.66	2.66	2.69	2.55
SRM-FE to PO_4-O1 (Å)	2.15	2.15	2.19	2.30
Fe_4S_4-FE4 to C483Sγ to SRM-FE (°)	127.5	127.1	126.4	121.7
C483Sγto SRM-FE to PO_4-O1 (°)	174.6	173.3	173.8	174.5
T477Cβ to Fe_4S_4-S2 (Å)	4.45	4.44	4.46	4.29
T477OH to Fe_4S_4-S2 (Å)	3.25	3.26	3.26	N/A
Fe_4S_4-FE4 to C483Sγ (Å)	2.27	2.26	2.26	2.32

the F437A variant, additional ordered solvent molecules appeared and filled the resulting cavities, solvating the backbone that had previously been shielded by the hydrophobicity of the Phe substituents (Fig. 4). Altering amino acid 437 to an alanine allows encroachment of three waters with refined occupancies of 1 and B-factors of 23 Å^3, 38 Å^3, and 37 Å^3 that fill the space and solvate the backbone of this loop.

One unique feature of the SiRHP active site is the disparity in the length of the bond between the bridging C483Sγ and the siroheme iron – 2.7 Å in the WT enzyme – and the bond between the siroheme iron and the oxygen of the distal-bound PO_4^{2-} – 2.2 Å in the WT structure. Such asymmetry in the axial bond lengths at the siroheme iron creates a rhombic distortion, which explains the characteristic EPR spectrum of oxidized SiRHP [13]. Neither the F437A nor M444A variation alters this geometry (Table 2). In contrast, T477A shows a shorter C483Sγ-SRM-Fe bond (2.6 Å) and a longer SRM-Fe – O-PO_4^{2-} bond (2.3 Å).

3.4. EPR analysis of the siroheme cofactor

One aspect of SiRHP function that was resolved from determining its three-dimensional structure was the nature of the exchange-coupled siroheme-Fe_4S_4 cluster cofactors [13,26,27], which are covalently bound through a common cysteine ligand that is both a proximal siroheme iron ligand and one of the coordinating cysteines to the Fe_4S_4 cluster [2]. Given the extended effects of the metallic cofactors, we asked if alteration to the environment of the Fe_4S_4 cluster affected the state of the $S = 5/2$ Fe^{3+}, as assessed by EPR spectroscopy.

The EPR signature for WT SiRHP at the experimental conditions specified above compares well to the expected signature, with turning points appearing at g = 6.69, 5.26 and 1.98 indicative of a rhombic distortion in a high spin, Fe^{3+} iron (Fig. 5). Neither the F437A nor M444A alteration significantly affected the EPR signal of the siroheme. In marked, although subtle, contrast, the EPR signal from the T477A variant varied reproducibly across repeated protein preparations. Specifically, we measured diminished splitting of the perpendicular turning points corresponding to a decrease in rhombicity from g = 6.69/5.26 to g = 6.62/5.33. The effect is repeatable and not dependent on temperature or power in the parameter range 10–20 K, 10–20 dB.

3.5. UV–Vis spectroscopic analysis of oxidized and reduced, CN^--bound SiRHP

We next wanted to assess the effect of the amino acid alterations on SiRHP's capacity to bind a distal ligand. We monitored CN^- binding to $2e^-$ reduced SiRHP because CN^- is a strong field ligand that traps a

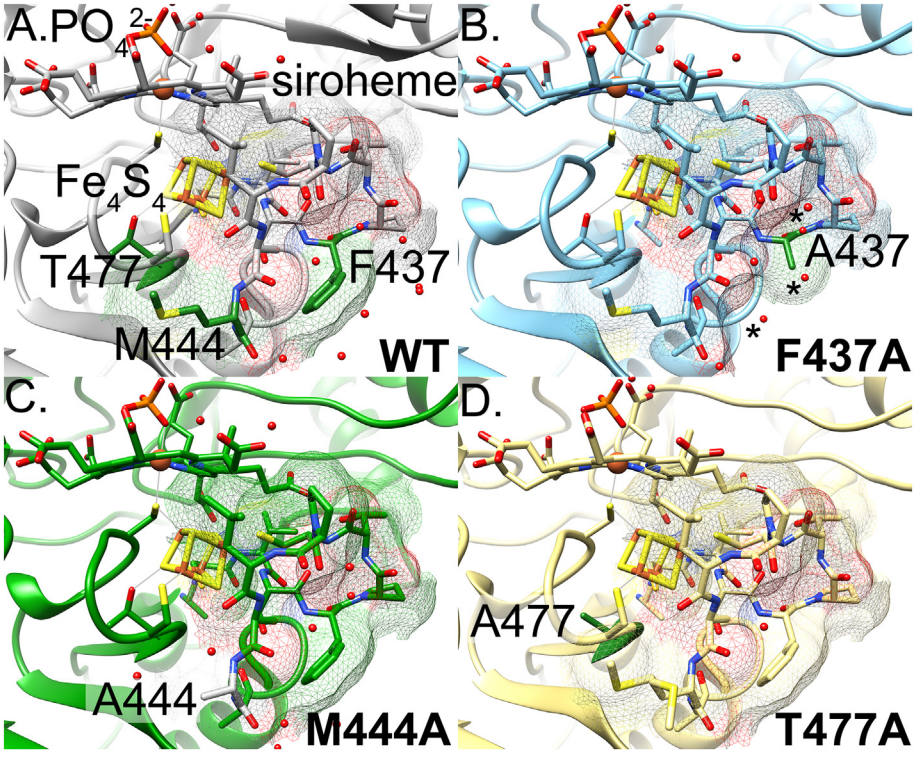

Fig. 4. X-ray crystallographic analysis of each variant shows little effect on the overall active site architecture. The first cluster loop is drawn as sticks as are the amino acids we altered and the cofactors. The rest of the structure is shown as a ribbon diagram. The solvent accessible surface is drawn as mesh. Water molecules that change as a result of the amino acid alteration are marked by an asterisk (*). A. WT, amino acids with their native identities. B. F437A, amino acid 437 labeled as an alanine. C. M444A, amino acid 444 labeled as an alanine. D. T477A, amino acid 477 labeled as an alanine.

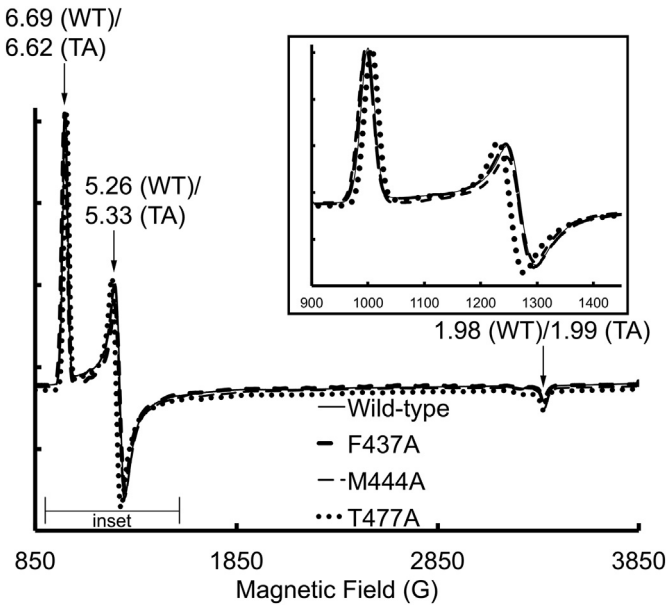

Fig. 5. X-band EPR spectra of oxidized SiRHP at 10 K and 10 dB (main plot) with the perpendicular region magnified in the inset. Neither the F437A nor M444A variants affect the spectrum of the siroheme Fe^{3+} but the T477A variant reduces the splitting of the perpendicular turning points from g = 6.69/5.26 to g = 6.62/5.33. The bracket indicates the region of the inset.

low-spin siroheme [30], assessed by the Soret and Q-bands. CN^- stabilizes and shortens the bonds between the iron and its proximal or distal ligand by drawing electrons into the coupled prosthetic groups [28] so is a measure of ligand binding. Exogenous ligands do not bind rapidly to oxidized SiRHP so it must be reduced to induce reduction-gated loss of the bound PO_4^{2-} [25]. Therefore, we measured the oxidized and reduced, CN^--bound UV–Vis spectra and compared the Soret (387 nm) and Q (590 nm) absorption bands (Fig. 6). In the oxidized spectra, each of the altered SiRHP variants showed a slight reduction in the intensity of the Soret band but near perfect overlap of the Q-band, suggesting that the enzyme has full cofactor occupancy. Upon CN^- binding, each variant behaves like WT, with a blue shift of the Soret band to 405 nm and a red shift of the Q-band to 580 nm.

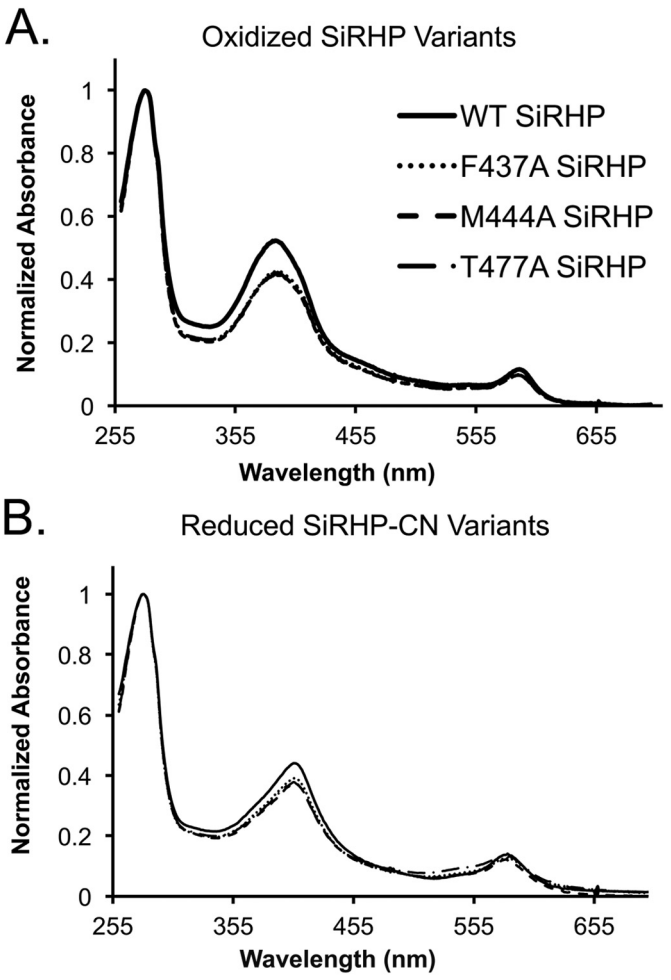

Fig. 6. UV–Vis analysis of SiRHP both oxidized and bound to a strong-field ligand shows that the strong-field ligand binds in a similar manner to all SiRHP variants. A. Oxidized and PO_4^{2-}- bound SiRHP variants. B. Reduced and CN^--bound SiRHP variants. The legend is the same for both panels.

4. Discussion

4.1. SiRHP's second shell ligands control access to its Fe4S4 cluster

F437 is a solvent-exposed amino acid on the first Fe_4S_4 cluster loop, which sits between the Fe_4S_4 ligands C434 and C440. The plane of the phenylalanine ring is 7 Å away from the closest Fe_4S_4 sulfide, with the methyl from A443 sitting nearly equidistance between the two. In this way, the side chain of F437 sits directly in line with a corner of the Fe_4S_4 cubane and, therefore, was initially proposed to play either a role in electron transfer or in subunit-subunit interactions [2]. The geometry of the first cluster loop is constrained by the strained S436 and the *cis*-P438, which together facilitate the outward orientation of the F437 side chain. Removing the phenyl ring through alteration to alanine does not relieve the strain but it does cause reordering of the solvent molecules that interact with the surface of the first cluster loop (Fig. 4).

Hydrogen-deuterium exchange and truncation analysis have previously showed that the N-terminal 80 amino acids of SiRHP is the structural element responsible for tight subunit-subunit binding of SiRHP with SiRFP [10]. Further, the F437A variant binds SiRFP-43 equally well in our gel shift analysis (Fig. 3B) and the holoenzyme preparation has an $\alpha_8\beta_4$ stoichiometry, as in WT SiR (Fig. 3A). These results support the idea that F437 does not play a role in holoenzyme assembly, as previously proposed [2]. Additionally, the EPR spectrum of F437A SiRHP is similar to WT (Fig. 5), suggesting that increased solvent accessibility does not alter the electronic configuration of the coupled siroheme-Fe_4S_4 cluster. In contrast, F437A shows enhanced reactivity to SO_3^{2-}, when either reduced chemically or by NADPH through its reductase partner (Table 2). This result suggests that in the absence of the bulky sidechain, the reductant, whether MV^+ or the flavin cofactor bound to the flavodoxin domain of SiRFP, has better access to first cluster loop, allowing for more rapid electron transfer. In this way, the phenyl group of F437 serves as a gate to control access to the enzyme's metallic cofactors but is not required as an intermediate for electron transfer.

M444 also contributes to the solvent-accessible surface near the Fe_4S_4 cluster, stacking against the Fe_4S_4 cluster ligand C479 – M444Cγ is 3.8 Å away from C479Cβ (Fig. 4). As in the F437A variant, altering this bulky sidechain to an alanine enhances electron transfer when the electrons are donated from a chemical reductant to the monomeric SiRHP (Table 2). In contrast, in the context of the holoenzyme, M444A activity is reduced, resulting in a lower rate of NADPH oxidation *in vitro* (Table 2) and smaller colony size *in vivo* (Fig. 2). M444A-SiRFP-43 binding is not affected by this variation (Fig. 3) so the reduced activity of the holoenzyme does not come from a defect in complex assembly. However, a transient interaction that modulates electron transfer from SiRFP to the siroheme must occur, in analogy to the cytochrome *p*450-cytochrome *p*450 reductase interaction [29], and it is possible that M444 plays a role either in positioning SiRFP for productive electron transfer or as an intermediate along the way to the siroheme.

4.2. Hydrogen bonds to the Fe_4S_4 cluster control the geometry at the siroheme iron

None of the point variants dramatically altered the structure of the active site and its surrounding regions (Fig. 4). The cysteine ligands to the Fe_4S_4 cluster from the WT, F437A, and M444A differ in their position by < 0.07 Å across the three X-ray crystal structures. In contrast, small but measurable changes (~0.2 Å) in the position of the cysteine ligands to the Fe_4S_4 cluster appeared in the X-ray crystallographic structure of the T477A variant, altering the geometry of the active site. Specifically, the bond between C483Sγ and the siroheme iron is ~2.7 Å in each of the WT, F437A, and M444A structures (average of 2.67 ± 0.02 Å). In the T477A structure, this distance is reduced to 2.55 Å. The siroheme iron to PO_4^{2-} distance is ~2.2 Å in the WT, F437A, and M44A structures (an average of 2.16 ± 0.02 Å) but the same bond is 2.3 Å long in the T477A structure.

Given the slightly lower resolution of the T477A structure than the others, we wanted to confirm that these changes were significant. EPR spectra of oxidized SiRHP show three turning points at g = 6.69, g = 5.26, and g = 1.98, consistent with a rhombically distorted porphyrinoid-type high spin iron ($S = 5/2$). The EPR spectra for WT, F437A, and M444A were superimposable. In contrast, in the T477A variant the three turning points were at g = 6.62, 5.33, and 1.99, suggesting an $S = 5/2$ Fe^{3+} with somewhat less geometric distortion, consistent with the small but measurable changes in the axial bond lengths for the siroheme iron. Interestingly, T477A also shows an enhanced electron transfer rate, regardless of its electron sources, suggesting that the distortions to the iron coordination do not inhibit enzyme activity. In fact, lengthening of the siroheme iron – substrate bond may help speed substrate release and, in this way, enhance enzyme activity.

4.3. SiR has properties distinct form DSRs

One difference between assimilatory SiRs and DSRs is that SiRs reduce sulfite fully, without releasing partially-reduced intermediates. In contrast, DSRs can release off pathway products like thiosulfate ($S_2O_3^{2-}$) and trithionite ($S_3O_6^{2-}$) [30]. The evolutionary driver of this difference is easily explained. Assimilatory SiRs synthesize a building block of other biomolecules so their importance lies in the product of their chemical reaction. In contrast, DSRs serve as the terminal electron acceptor in sulfur-based respiration so their importance lies in building the proton motive force to ultimately synthesize ATP. The biophysical forces that underlie this difference are less clear but the consequence is that sulfite binds siroheme differently in SiRHP than in DSR [28,30]. Here, we identified three amino acids with varying conservation patterns across the different sulfite reductases (Fig. 1B). Specifically, F437 is a bulky amino acid in assimilatory SiRs but not in DSRs. M444 is a charged or hydrophobic amino acid in ferredoxin-dependent assimilatory SiRs but a cysteine in DSRs. T477 is a small, polar amino acid in assimilatory SiRs but an aspartic acid – or even an alanine, as we made in our study, in DSRs. Given this wide range, the amino acids that we identified to control access to the multi-iron prosthetic group and govern ligand binding at the distal face of the siroheme may also contribute to SiRHP's more effective reduction of sulfite.

The process of reducing sulfur has potential to cause damage to cells because partially-reduced, reactive sulfur species (RSS) can interact with reactive oxygen species (ROS) and the free radical signaling molecule nitric oxide (NO) to trigger redox stress [31]. Interestingly, despite the enhanced activity of F437A and T477A variants measured in the SiR dodecamer, none of the point variants resulted in more robust complementation of a SiRHP deletion (Fig. 2). One interpretation of this observation could be that the enhanced enzyme activity of the SiRHP harboring these amino acid alterations leads to an increased amount of reduced sulfur, perhaps in the form of partially-reduced sulfur species like DSRs can produce, that are toxic to *E. coli*. In this way, NADPH-dependent SiRHP has evolved so that its activity is optimized for the health of the overall organism and not simply to maximize enzyme efficiency.

5. Conclusions

We have endeavored to dissect the molecular interactions that modulate electron transfer in the multi-iron active site of SiRHP. We discovered that two bulky sidechains, F437 and M444, serve as gates to the active site because both the F437A and M444A variants are more reactive when reduced chemically, likely because the chemical reductant has superior access to the active site. In contrast, the F437A variant is also more active as part of the dodecamer but the M444A variant is not. This contrasting result suggests that M444, but not F437, plays a role in electron transfer from its endogenous reductase partner. T477, which makes a hydrogen bond with the Fe_4S_4 cluster, also affects the rhombic distortions of the siroheme iron. Removing that interaction lengthens the Fe^{3+}-PO_4^{2-} bond length, suggesting that this variant's enhanced activity when chemically reduced or as part of the SiR dodecamer may arise from a weakening of the Fe-substrate interaction.

Acknowledgements

This work was supported by National Science Foundation award MCB1149763 to MES and a National Science Foundation Graduate Research Fellowship to JMP. A portion of this work was performed at the National High Magnetic Field Laboratory, which is supported by National Science Foundation Cooperative Agreement No. DMR-1157490 and the State of Florida. We thank Dr. A. Ozarowski for his software package SPIN. The coordinates and structure factors for the X-ray crystal structures have been deposited to the RCSB under the following PDB IDs: WT (PDB ID: 6C3M), F437A (PDB ID: 6C3X), M444A (PDB ID: 6C3Y), and T477A (6C3Z).

MRC and LM performed the biochemical analysis. LM grew the protein crystals and JMP collected the X-ray crystallographic data. JK performed the EPR experiments. MES designed and oversaw the study, refined the X-ray crystal structures, assisted in acquisition of the EPR data, acquired funding, and wrote the manuscript.

References

[1] B.R. Crane, E.D. Getzoff, The relationship between structure and function for the sulfite reductases, Curr. Opin. Struct. Biol. 6 (6) (1996) 744–756.
[2] B.R. Crane, L.M. Siegel, E.D. Getzoff, Sulfite reductase structure at 1.6 A: evolution and catalysis for reduction of inorganic anions, Science 270 (5233) (1995) 59–67.
[3] K.D. Bewley, K.E. Ellis, M.A. Firer-Sherwood, S.J. Elliott, Multi-heme proteins: nature's electronic multi-purpose tool, Biochim. Biophys. Acta 1827 (8–9) (2013) 938–948.
[4] B. Hermann, M. Kern, L. La Pietra, J. Simon, O. Einsle, The octahaem MccA is a haem c-copper sulfite reductase, Nature 520 (7549) (2015) 706–709.
[5] E.F. Johnson, B. Mukhopadhyay, Coenzyme F420-dependent sulfite reductase-enabled sulfite detoxification and use of sulfite as a sole sulfur source by *Methanococcus maripaludis*, Appl. Environ. Microbiol. 74 (11) (2008) 3591–3595.
[6] M. Goujon, H. McWilliam, W. Li, F. Valentin, S. Squizzato, J. Paern, R. Lopez, A new bioinformatics analysis tools framework at EMBL-EBI, Nucleic Acids Res. 38 (Web Server) (2010) W695–W699.
[7] F. Sievers, D.G. Higgins, Clustal Omega for making accurate alignments of many protein sequences, Protein Sci. 27 (1) (2018) 135–145.
[8] L.M. Siegel, M.J. Murphy, H. Kamin, Reduced nicotinamide adenine dinucleotide phosphate-sulfite reductase of enterobacteria. I. The *Escherichia coli* hemoflavoprotein: molecular parameters and prosthetic groups, J. Biol. Chem. 248 (1) (1973) 251–264.
[9] L.M. Siegel, P.S. Davis, Reduced nicotinamide adenine dinucleotide phosphate-sulfite reductase of enterobacteria. IV. The *Escherichia coli* hemoflavoprotein: subunit structure and dissociation into hemoprotein and flavoprotein components, J. Biol. Chem. 249 (5) (1974) 1587–1598.
[10] I. Askenasy, J.M. Pennington, Y. Tao, A.G. Marshall, N.L. Young, W. Shang, M.E. Stroupe, The N-terminal domain of *Escherichia coli* assimilatory NADPH-sulfite reductase hemoprotein is an oligomerization domain that mediates holoenzyme assembly, J. Biol. Chem. 290 (31) (2015) 19319–19333.
[11] T.F. Oliveira, C. Vonrhein, P.M. Matias, S.S. Venceslau, I.A. Pereira, M. Archer, The crystal structure of *Desulfovibrio vulgaris* dissimilatory sulfite reductase bound to DsrC provides novel insights into the mechanism of sulfate respiration, J. Biol.

Chem. 283 (49) (2008) 34141–34149.
[12] K.W. Smith, M.E. Stroupe, Mutational analysis of sulfite reductase hemoprotein reveals the mechanism for coordinated electron and proton transfer, Biochemistry 51 (49) (2012) 9857–9868.
[13] P.A. Janick, L.M. Siegel, Electron paramagnetic resonance and optical spectroscopic evidence for interaction between siroheme and Fe4S4 prosthetic groups in *Escherichia coli* sulfite reductase hemoprotein subunit, Biochemistry 21 (15) (1982) 3538–3547.
[14] L.M. Siegel, D.C. Rueger, M.J. Barber, R.J. Krueger, N.R. Orme-Johnson, W.H. Orme-Johnson, Escherichia coli sulfite reductase hemoprotein subunit. Prosthetic groups, catalytic parameters, and ligand complexes, J. Biol. Chem. 257 (11) (1982) 6343–6350.
[15] P.A. Janick, D.C. Rueger, R.J. Krueger, M.J. Barber, L.M. Siegel, Characterization of complexes between *Escherichia coli* sulfite reductase hemoprotein subunit and its substrates sulfite and nitrite, Biochemistry 22 (2) (1983) 396–408.
[16] J.Y. Wu, L.M. Siegel, N.M. Kredich, High-level expression of *Escherichia coli* NADPH-sulfite reductase: requirement for a cloned cysG plasmid to overcome limiting siroheme cofactor, J. Bacteriol. 173 (1) (1991) 325–333.
[17] H. Liu, J.H. Naismith, An efficient one-step site-directed deletion, insertion, single and multiple-site plasmid mutagenesis protocol, BMC Biotechnol. 8 (2008) 91.
[18] T. Baba, T. Ara, M. Hasegawa, Y. Takai, Y. Okumura, M. Baba, K.A. Datsenko, M. Tomita, B.L. Wanner, H. Mori, Construction of *Escherichia coli* K-12 in-frame, single-gene knockout mutants: the Keio collection, Mol. Syst. Biol. 2 (2006) (2006) 0008.
[19] C.A. Schneider, W.S. Rasband, K.W. Eliceiri, NIH image to ImageJ: 25 years of image analysis, Nat. Methods 9 (7) (2012) 671–675.
[20] J. Schindelin, C.T. Rueden, M.C. Hiner, K.W. Eliceiri, The ImageJ ecosystem: an open platform for biomedical image analysis, Mol. Reprod. Dev. 82 (7–8) (2015) 518–529.
[21] L.M. Siegel, P.S. Davis, H. Kamin, Reduced nicotinamide adenine dinucleotide phosphate-sulfite reductase of enterobacteria. 3. The *Escherichia coli* hemoflavoprotein: catalytic parameters and the sequence of electron flow, J. Biol. Chem. 249 (5) (1974) 1572–1586.
[22] P. Emsley, B. Lohkamp, W.G. Scott, K. Cowtan, Features and development of Coot, Acta Crystallogr. D Biol. Crystallogr. 66 (Pt 4) (2010) 486–501.
[23] P.D. Adams, P.V. Afonine, G. Bunkoczi, V.B. Chen, I.W. Davis, N. Echols, J.J. Headd, L.W. Hung, G.J. Kapral, R.W. Grosse-Kunstleve, A.J. McCoy, N.W. Moriarty, R. Oeffner, R.J. Read, D.C. Richardson, J.S. Richardson, T.C. Terwilliger, P.H. Zwart, PHENIX: a comprehensive python-based system for macromolecular structure solution, Acta Crystallogr. D Biol. Crystallogr. 66 (Pt 2) (2010) 213–221.
[24] T. Beitlich, K. Kühnel, C. Schulze-Briese, R.L. Shoeman, I. Schlichting, Cryoradiolytic reduction of crystalline heme proteins: analysis by UV-Vis spectroscopy and X-ray crystallography, J. Synchrotron Radiat. 14 (Pt 1) (2007) 11–23.
[25] B.R. Crane, L.M. Siegel, E.D. Getzoff, Structures of the siroheme- and Fe4S4-containing active center of sulfite reductase in different states of oxidation: heme activation via reduction-gated exogenous ligand exchange, Biochemistry 36 (40) (1997) 12101–12119.
[26] J.A. Christner, E. Munck, P.A. Janick, L.M. Siegel, Mossbauer spectroscopic studies of *Escherichia coli* sulfite reductase. Evidence for coupling between the siroheme and Fe4S4 cluster prosthetic groups, J. Biol. Chem. 256 (5) (1981) 2098–2101.
[27] J.A. Christner, E. Munck, P.A. Janick, L.M. Siegel, Mossbauer evidence for exchange-coupled siroheme and [4Fe-4S] prosthetic groups in *Escherichia coli* sulfite reductase. Studies of the reduced states and of a nitrite turnover complex, J. Biol. Chem. 258 (18) (1983) 11147–11156.
[28] B.R. Crane, L.M. Siegel, E.D. Getzoff, Probing the catalytic mechanism of sulfite reductase by X-ray crystallography: structures of the *Escherichia coli* hemoprotein in complex with substrates, inhibitors, intermediates, and products, Biochemistry 36 (40) (1997) 12120–12137.
[29] Y. Farooq, G.C.K. Roberts, Kinetics of electron transfer between NADPH-cytochrome P450 reductase and cytochrome P450 3A4, Biochem. J. 432 (2010) 485–493.
[30] K. Parey, E. Warkentin, P.M. Kroneck, U. Ermler, Reaction cycle of the dissimilatory sulfite reductase from *Archaeoglobus fulgidus*, Biochemistry 49 (41) (2010) 8912–8921.
[31] C. Jacob, A. Anwar, The chemistry behind redox regulation with a focus on sulphur redox systems, Physiol. Plant. 133 (3) (2008) 469–480.